



Preparation and antibacterial activity of Zn coating on pure Ti with enhanced adhesion

Ming Li^a, Qiang Li^{a,b,*}, Jiawei Yang^a, Mitsuo Niinomi^{a,c,d}, Takayoshi Nakano^d

^a School of Mechanical Engineering, University of Shanghai for Science and Technology, Shanghai 200093, PR China

^b Shanghai Engineering Research Center of High-Performance Medical Device Materials, Shanghai 200093, PR China

^c Institute for Materials Research, Tohoku University, 2-1-1, Katahira, Aoba-ku, Sendai 980-8577, Japan

^d Division of Materials and Manufacturing Science, Graduate School of Engineering, Osaka University, 2-1, Yamada-Oka, Suita, Osaka 565-0871, Japan

ARTICLE INFO

Keywords:

Zn-containing coating
Electrochemical deposition
Orthogonal experiment
Adhesion
Antibacterial property
Pure Ti

ABSTRACT

A titania nanotubes layer was prepared as an intermediate layer on pure Ti via anodic oxidation, and subsequently, a Zn-containing coating was electrochemically deposited. The influence of the deposition parameters on the Zn content was studied using an orthogonal experiment. The obtained coatings were characterized using scanning electron microscopy, energy-dispersive spectroscopy, X-ray diffraction, and X-ray photoelectron spectroscopy, and their adhesion was measured using a scratch test. The deposition time had the greatest effect on the Zn content of the electrodeposited samples, whereas the deposition temperature had the smallest effect. After the electrodeposition, Zn was uniformly distributed on the surface and existed mainly as a simple substance. The adhesion was only 10.9 N in the Zn-free sample; it increased with increasing Zn content of the samples, and reached a maximum value of 22.4 N in the sample with a Zn content of approximately 16%. The samples with Zn-containing coatings exhibited strong antibacterial effects against *E. coli* and *S. aureus*, and the antibacterial effect increased with increasing Zn content. Cell viability was above 80%, indicating that the Zn-containing coating is a good candidate as an antibacterial coating for biomedical applications.

1. Introduction

Ti and its alloys have been widely used in dental and orthopedic implants owing to their excellent mechanical properties, good corrosion resistance, and high biocompatibility [1]. However, some implant failures occur primarily because of peri-implant inflammation caused by bacterial infection, which significantly influences patient health and medical costs [2]. Therefore, bacterial infections can be reduced by endowing implants with antibacterial and osteogenic properties [3].

Several antiseptics have been loaded with surface modifications to enhance the antibacterial activity of implants. Natural antimicrobial agents were first used on humans. Their sources are mainly animal and plant bodies, which are highly compatible with living organisms [4]. However, their poor antimicrobial effects, low stability, and low long-lasting release considerably limit their widespread application in the biomedical field [5,6]. Organic antimicrobial coatings containing antibiotics, such as vancomycin and gentamicin, exhibit effective antimicrobial effects [7,8]; however, antibiotics have a limited range of activity and may induce antibiotic resistance [9]. Nonantibiotic organic

antibacterial agents have overcome these drawbacks. For example, chlorhexidine is widely used in dentistry and can be easily adsorbed onto unmodified surfaces, which is clinically relevant [10]. However, several reports have indicated that nonantibiotic organic antimicrobial agents may cause cell damage [11,12]. Inorganic antimicrobial agents possess several advantages, such as high antibacterial activity and satisfactory stability [10]. Ag-doped calcium TiO₂ coatings exhibit high antibacterial activity [13]; however, Ag is expensive and cytotoxic. Silver nanoparticles have been shown to impair cellular mitochondria and lysosomes, and the potential mechanisms involved in oxidative stress, autophagy, and apoptosis are via the PI3K/AKT/mTOR signaling pathway [14]. Zn is an essential trace element in human bone, and plays crucial roles in growth, protein synthesis, and cell proliferation [15]. Zn can promote the osteogenic function of osteoblasts by stimulating cell proliferation, alkaline phosphatase activity, collagen synthesis, and protein synthesis [16–18], and enhances the expression of osteoblast marker genes [19]. In addition, when used as an antibacterial agent, Zn exhibits several advantages, such as safety, fewer side effects, and long-lasting antibacterial effects.

* Corresponding author at: School of Mechanical Engineering, University of Shanghai for Science and Technology, Shanghai 200093, PR China.

E-mail addresses: jqli@tju.edu.cn, liqiang@usst.edu.cn (Q. Li).

<https://doi.org/10.1016/j.mtcomm.2024.108149>

Received 19 September 2023; Received in revised form 16 December 2023; Accepted 16 January 2024

Available online 23 January 2024

2352-4928/© 2024 Elsevier Ltd. All rights reserved.

Numerous techniques, such as physical vapor deposition, chemical vapor deposition, sol-gel, and electrochemical deposition, have been employed to deposit coatings [20–22]. Among these, electrochemical deposition is an increasingly popular and frequently used approach, owing to its simplicity, ease of parameter control, uniform coating thickness, and applicability to multidimensional implant surfaces [23]. Electrochemical deposition allows good control over coating properties, such as crystal structure, micro/nanostructure, and composition, and provides flexibility for designing and producing several features, such as ion-substituted coatings on biomedical metal substrates [24]. However, the adhesion of directly deposited coatings is relatively low [25]. Nanostructured TiO₂ has been demonstrated to improve the adhesion properties of the substrate considerably and promote bone cell functionality in vitro [26] and bone implant osseointegration in vivo [27].

In this study, a titania nanotubes (TNs) layer was prepared as an intermediate layer on a pure Ti surface via anodic oxidation, and Zn-containing coatings were electrochemically deposited. The surface characteristics, antibacterial properties, and cell compatibility of the prepared coatings were also investigated.

2. Materials and methods

2.1. Preparation and anodization

Ti sheets (purity of 99.5%) with the dimensions of 10 × 10 × 1 mm³ were polished with 200–1200# sandpaper and then ultrasonically cleaned in each of acetone, anhydrous ethanol, and distilled water for 600 s. The sheets were acid-etched in a mixture of HF and HNO₃ (V_{HF}:V_{HNO₃}:V_{H₂O} = 1:3:10) for 30 s, ultrasonically cleaned in deionized water, and then dried in a drying oven at 60 °C.

For anodization, a double-electrode system was adopted, with a Ti sheet as the anode and a Pt sheet as the cathode; the distance between the two electrodes was 20 mm. Anodization was performed at a voltage of 30 V for 1 h in an ethylene glycol solution (V_{H₂O}:V_{CH₂OH} = 3:97) containing 0.3% NH₄F at room temperature (~25 °C). Subsequently, the sample was ultrasonically cleaned in ethanol and deionized water for 600 s, and then naturally dried in air. The anodized samples were denoted as TNs.

2.2. Electrodeposition

The electrolyte was prepared by dissolving ZnCl₂ (analytical pure) in deionized water. Pt and the TNs were used as the anode and cathode, respectively. The distance between the two electrodes was 20 mm, and the deposition voltage was 3 V. The beaker containing the electrolyte was placed in a water bath to maintain the deposition temperature. The electrodeposited samples were ultrasonically cleaned in deionized water for 600 s and dried naturally in air.

The effects of three selected factors—ZnCl₂ concentration in the electrolyte, deposition time, and temperature—on the Zn content of the samples were studied using orthogonal experiments. The factor levels of the orthogonal experiment are listed in Table 1, and an L₉(3³) orthogonal experiment table (Table 2) was constructed with the three factors and three levels using the Zn content of the electrodeposited sample as the evaluation index.

Table 1
Factor levels of the orthogonal experiment.

Level	Factor		
	ZnCl ₂ concentration / mol/L	Deposition time / s	Temperature / °C
1	0.02	20	30
2	0.04	40	40
3	0.06	60	50

Table 2
Orthogonal experiment scheme and results.

Number	ZnCl ₂ concentration / mol/L	Deposition time / s	Temperature / °C	Zn content / mass%
1	0.02	20	30	1.02
2	0.02	40	40	5.23
3	0.02	60	50	9.87
4	0.04	20	40	4.16
5	0.04	40	50	8.59
6	0.04	60	30	16.16
7	0.06	20	50	6.35
8	0.06	40	30	12.09
9	0.06	60	40	20.34

2.3. Characterizations of surface layer

The morphology was observed using scanning electron microscopy (SEM) at an acceleration voltage of 30 kV, and the chemical composition was analyzed using energy-dispersive spectroscopy (EDS). The phase composition was analyzed via X-ray diffraction (XRD) using Cu K α radiation at a voltage of 40 kV, a current of 40 mA, and a scanning speed of 4°/min. The chemical states of Ti and Zn were further analyzed using X-ray photoelectron spectroscopy (XPS) with a monochrome Al K α (h ν = 1486.6 eV) X-ray used as the radiation source. An automatic scratch tester containing a diamond indenter with a tip radius of 0.2 mm was used for the adhesion of the coatings under a vertically applied load of 40 N/min. After immersing the sample in a phosphate-buffered saline (PBS) solution at 37 °C for 24 h, the concentration of Zn²⁺ in the solution was detected using inductively-coupled plasma mass spectrometry.

2.4. Antibacterial test

Gram-negative *E. coli* (ATCC 25922) and gram-positive *S. aureus* (ATCC 29213) were selected for antibacterial performance testing. The antibacterial properties of the coatings were evaluated using a plate-counting method. After all the samples were sterilized at 121 °C for 20 min in an autoclave, they were added to a 24-well plate. The bacterial solution was diluted to 10⁶ CFU/mL with Luria–Bertani liquid medium, and 0.2 mL of the diluted bacterial solution was added to each sample surface. The 24-well plate was incubated at 37 °C for 18 h, and then the co-culture solution was diluted 10⁵ times with a sterile PBS solution. Then, 100 μ L diluent was evenly coated on the solid medium. After incubation at 37 °C in a constant-temperature incubator for 18 h, the colony number was recorded, and the antibacterial rate of each coated sample was calculated using a previously described formula [28].

2.5. Cytocompatibility test

MC3T3-E1 cells (iCell Bioscience Inc., Shanghai, China) were used to evaluate the cytotoxicity. α -MEM supplemented with 10% fetal bovine serum was used as the culture medium. All the samples were solid sheets with a surface area of 1 cm². After being sterilized under a high temperature and pressure, they were added to a complete medium (ISO 10993–12) at an extraction rate of 1.25 cm²/mL, and extraction was performed at 37 °C for 24 h. Each sample extract (100 μ L) was placed in separate 96-well plates, and three parallel wells were set up for each sample. The MC3T3-E1 cells were seeded in each well at a density of 6 × 10³ cells/well. The culture medium was removed after being incubated for 24, 96, and 168 h in a constant-temperature incubator at 37 °C in a 5% CO₂ atmosphere. Each well was rinsed three times with PBS. Then, 100 μ L of a culture medium containing 0.5 mg/mL MTT was added to each well, and then incubated in the constant-temperature incubator at 37 °C in a 5% CO₂ atmosphere for 4 h. The supernatant was discarded, 100 μ L of dimethyl sulfoxide was added to each well, and the absorbance was measured at 570 nm after shaking the mixture for 600 s.

3. Results and discussion

3.1. Characterization of TNs

The preparation and characterization of TNs have been extensively studied [29,30]. In this study, the surface morphology exhibits a uniformly distributed circular nanotube with a diameter of approximately 60 nm, as shown in Fig. 1a. The side-view suggested that the length of the TNs was approximately 2 μm (Fig. 1b). The characteristic peaks of Ti, O, F, C, and N were observed using XPS, as shown in Fig. 1c. The appearance of C and N is related to CO_2 and N_2 in air, respectively [31], whereas F is derived from the electrolyte solution during anodic oxidation [32]. A small amount of F ions can promote cell growth but hardly affect the antibacterial activity [33,34]. The binding energies of Ti 2p_{1/2} and Ti 2p_{3/2} are approximately 464.5 eV and 458.8 eV, respectively, matching the typical binding energies of TiO_2 [35]. The diffraction peaks of Ti were observed using XRD, as shown in Fig. 1d. No other diffraction peaks were observed, indicating that the layer was thin and the TNs were amorphous [36]. In situ anodized TNs can considerably improve the coating adhesion strength, and TNs with the diameters of 30–100 nm can promote the growth of osteoblasts, improve the surface biological activity, and form strong chemical bonds with bone [37–39]. Therefore, the prepared TNs are suitable as intermediate layers for the subsequent electrodeposition process.

3.2. Orthogonal experimental analysis

The Zn contents of the electrodeposited samples were determined using EDS, as shown in Table 2. Range analysis was used to calculate the averages (K₁, K₂, and K₃) and range values (R_K) of the Zn content in the coatings at each factor level, as shown in Table 3. The range reflects the

Table 3

Range analysis of the Zn content of the samples.

Calculated value	Factor		
	ZnCl ₂ concentration	Deposition time	Deposition temperature
K ₁	5.37	3.84	9.76
K ₂	9.64	8.64	9.91
K ₃	12.93	15.46	8.27
R _K	7.56	11.62	1.64

influence of various factors on the experimental indicators [40]. The range value of the deposition time was 11.62, which was greater than those of the ZnCl₂ concentration and deposition temperature. Therefore, the order of influence of the various factors on the Zn content was deposition time > ZnCl₂ concentration > deposition temperature. Subsequently, a variance analysis was conducted, as shown in Table 4. The smaller the significance value, the greater is the influence of the corresponding factors on the Zn content of the coating [41]. The deposition time showed the smallest significance value of less than 0.05, suggesting that it had the greatest influence on the Zn content. The deposition temperature had the smallest influence on the Zn content because its significance value was the highest and greater than 0.1. Good consistency was obtained in the range and variance analyses, which suggested that the deposition time had the greatest influence on the Zn content, and the deposition temperature had the smallest influence. Therefore, changing the deposition time and ZnCl₂ concentration is a feasible way to control the Zn content of the coating.

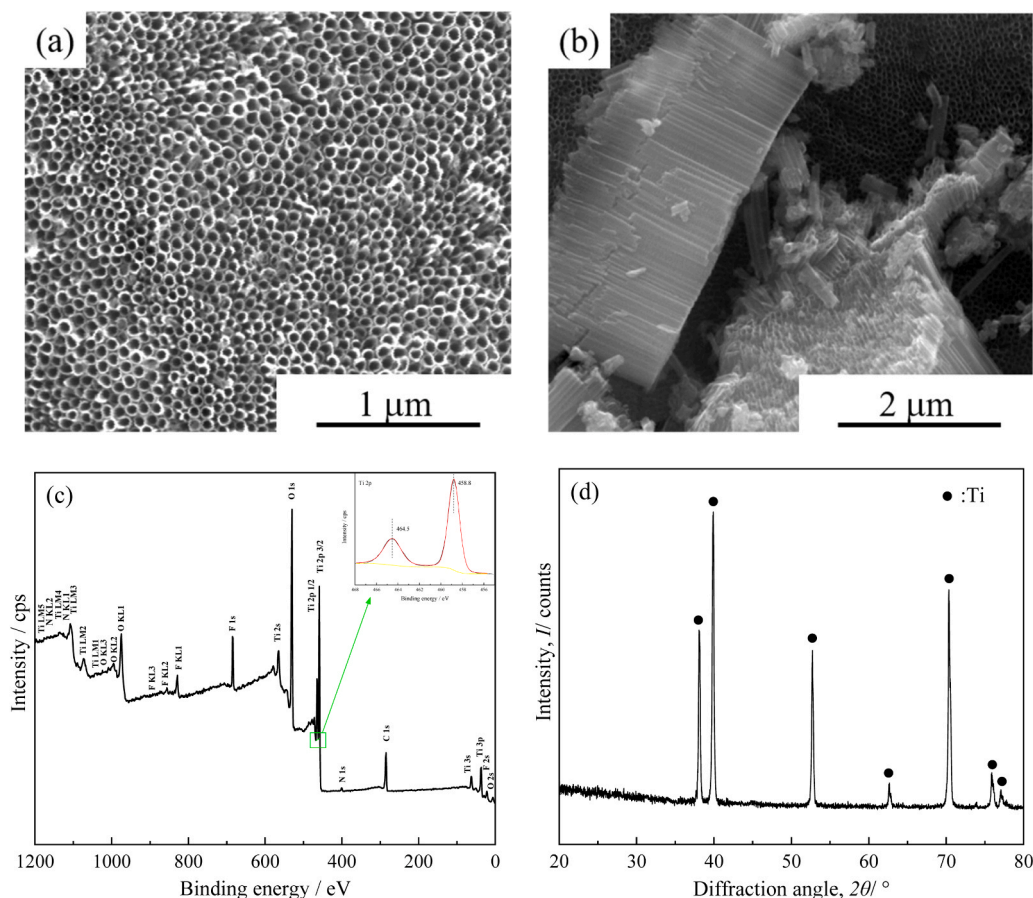


Fig. 1. Characterizations of the sample after anodic oxidation: (a) surface morphology, (b) side view of TNs, (c) XPS spectrum, and (d) XRD pattern.

Table 4
Variance analysis of the Zn content of the samples.

Variance source	Sum of squares of deviations	Free degree	Mean square	F-value	Conspicuousness
ZnCl ₂ concentration	86.053	2	43.026	34.922	0.028
Deposition time	204.358	2	102.179	82.932	0.012
Deposition temperature	4.923	2	2.462	1.998	0.334
Error	2.464	2	1.232		
Total	297.8	8			

3.3. Characterization of the coatings

To obtain a gradient variation in the Zn content, the electrodeposition parameters were set according to Table 5 together with the Zn contents measured using EDS. The sample with the lowest Zn content was named Zn-TNs-L, that with the highest Zn content was named Zn-TNs-H, and that with medium Zn content was named Zn-TNs-M. Surface morphologies were observed using SEM, as shown in Fig. 2. Small blocks were observed in all the samples under low magnification (Fig. 2a, c, and e). The high-magnification images suggest that a new layer grew around the walls of the TNs, covering the gaps between the nanotubes (Fig. 2b, d, and f). The separated nanotubes changed to a nanomesh structure, with the average diameter of the tubes decreasing to 48 nm. The nanomesh structure was similar to the shape of natural human bone and facilitated osteoblast growth [42].

The elemental distribution of Zn-TNs-L is shown in Fig. 3. Ti, O, Cl, and Zn were uniformly distributed on the surface of the sample (Fig. 3b), and the segregation of Zn was hardly observed (Fig. 3c). As shown in the side-view image (Fig. 3d), the tops of the TNs were partially dissolved, and the electrodeposited coating was formed mainly around the top area. The elemental distribution in the side view shows that the elements were uniformly distributed from the bottom to the top of the TNs (Fig. 3e), suggesting that electrodeposition also occurred inside the TNs besides the top of the TNs.

The XPS and XRD spectra of Zn-TNs-L, Zn-TNs-M, and Zn-TNs-H are shown in Fig. 4. Peaks corresponding to Ti, O, Zn, C, N, and F were observed in the full spectrum (Fig. 4a). Compared with Fig. 3c, the appearance of the Zn peaks also proves that Zn was successfully deposited. The high-resolution spectra of Zn2p (Fig. 4b) show that the binding energies of Zn2p_{3/2} and Zn2p_{1/2} were located near 1021.8 eV and 1044.9 eV, respectively, which correspond to Zn²⁺ of ZnO [43]. Only the diffraction peaks of Ti were observed in the XRD pattern of Zn-TNs-L (Fig. 4c), which was similar to that of the TNs (Fig. 1d). Beside the Ti peaks, the weak peaks corresponding to Zn around the 2θ of 36.19° and 43.17° were observed in the XRD pattern of Zn-TNs-M, and the peaks became sharper and stronger in the XRD pattern of Zn-TNs-H, indicating an increase in the Zn content and its crystallinity. The diffraction peak of the Zn compound was barely observed in the XRD spectra, indicating that Zn mainly existed as a simple substance in the Zn-containing coatings. The chemical reaction for the deposition process is Zn²⁺ + 2e⁻ → Zn. The XRD results were inconsistent with the XPS results because they suggested that Zn existed in the form of ZnO. The detection depth of XRD is usually greater than 10 μm, and the substrate can be detected [44]. Thus, the Ti substrate and a certain amount of Zn in the

Table 5
Deposition parameters and Zn contents of different Zn-containing coatings.

Sample	ZnCl ₂ concentration / mol/L	Deposition time / s	Deposition temperature / °C	Zn content / mass%
Zn-TNs-L	0.04	30	30	4.84
Zn-TNs-M	0.06	30	30	10.62
Zn-TNs-H	0.04	60	30	16.16

coatings exhibited diffraction peaks in their XRD patterns. However, the detection depth of XPS is 5–10 nm, and the chemical states of the surface atoms can be determined [45]. ZnO is usually formed on the Zn surface in air according to the chemical reaction 2Zn + O₂ → 2ZnO [46]. Therefore, both Ti⁴⁺ and Zn²⁺ were detected via XPS, whereas Ti and Zn were hardly detected as simple substances.

Owing to the disordered nature of the amorphous states, the Zn–O bonds in the surface amorphous layer of the coating were relatively weaker than those in crystalline ZnO [47]. The solubility of ZnO is much higher than that of the simple substance Zn, and the Zn–O bond can induce the formation of reactive oxide species (ROS) on the surface of ZnO [48]. Therefore, the weak Zn–O bond in amorphous ZnO is not only the main contributor to the release of Zn²⁺ from Zn-containing coatings, but also the producer of ROS, which is beneficial for enhancing the antibacterial performance of the coatings.

3.4. Adhesiveness

The scratch method was used to determine the adhesion between the coating and the substrate. The variations in the friction and acoustic signals with respect to the applied load are shown in Fig. 5. At the beginning of the scratch, the friction increased linearly with an increase in the load. When the indenter contacted the substrate, the friction force suddenly increased as the slope of the curve increased and noise was generated, suggesting that the coating had peeled off. The corresponding load was regarded as the critical load. The applied load corresponding to the first acoustic peak in Fig. 5a was recorded as the bonding force of the TNs, which was approximately 10.9 N. However, the acoustic peak was hardly generated in the samples with the Zn-containing coating because the coating became soft after the deposition of Zn [49]. The bonding force of the Zn content was then determined by judging the inflection point of the slope of the friction curve (Fig. 5b, c, and d). As the Zn content increased, the bonding force and corresponding friction also increased, which is consistent with Gao's results [50]. The Zn coating was predominantly physically bonded to the TNs. The reinforcement of the cohesive strength of Zn with TNs as a roughened surface provides a more compatible scaffolding for adhesion via mechanical interlocking compared with the available conventional smooth surface. Additionally, as Zn was deposited not only on the top of TNs but also along the TNs with the gaps filled, the increase in Zn content led to a denser coating with improved adhesion properties. The bonding force of Zn-TNs-H (22.4 N) was higher than those of Zn-TNs-L and Zn-TNs-M.

3.5. Antibacterial properties

The Zn²⁺ concentration of the samples after immersion in the PBS solution for 24 h is shown in Fig. 6a. The increase in Zn²⁺ concentration suggests that the release amount of Zn²⁺ increased with increasing Zn content in the coating. It has been indicated that 10 ppm Zn²⁺ causes 50% of cell death [51] and the optimal concentration range of Zn²⁺ is 10⁻⁴–10⁻⁶ mol/L (6.5–650 μg/L), which ensures both antibacterial properties and little damage to mammalian cells [52]. The amount of Zn released from all the prepared samples was not only within the safe range but also within the optimal concentration range.

The antibacterial properties of CP-Ti, Zn-TNs-L, Zn-TNs-M, and Zn-TNs-H against *E. coli* and *S. aureus* are shown in Fig. 6b. A large

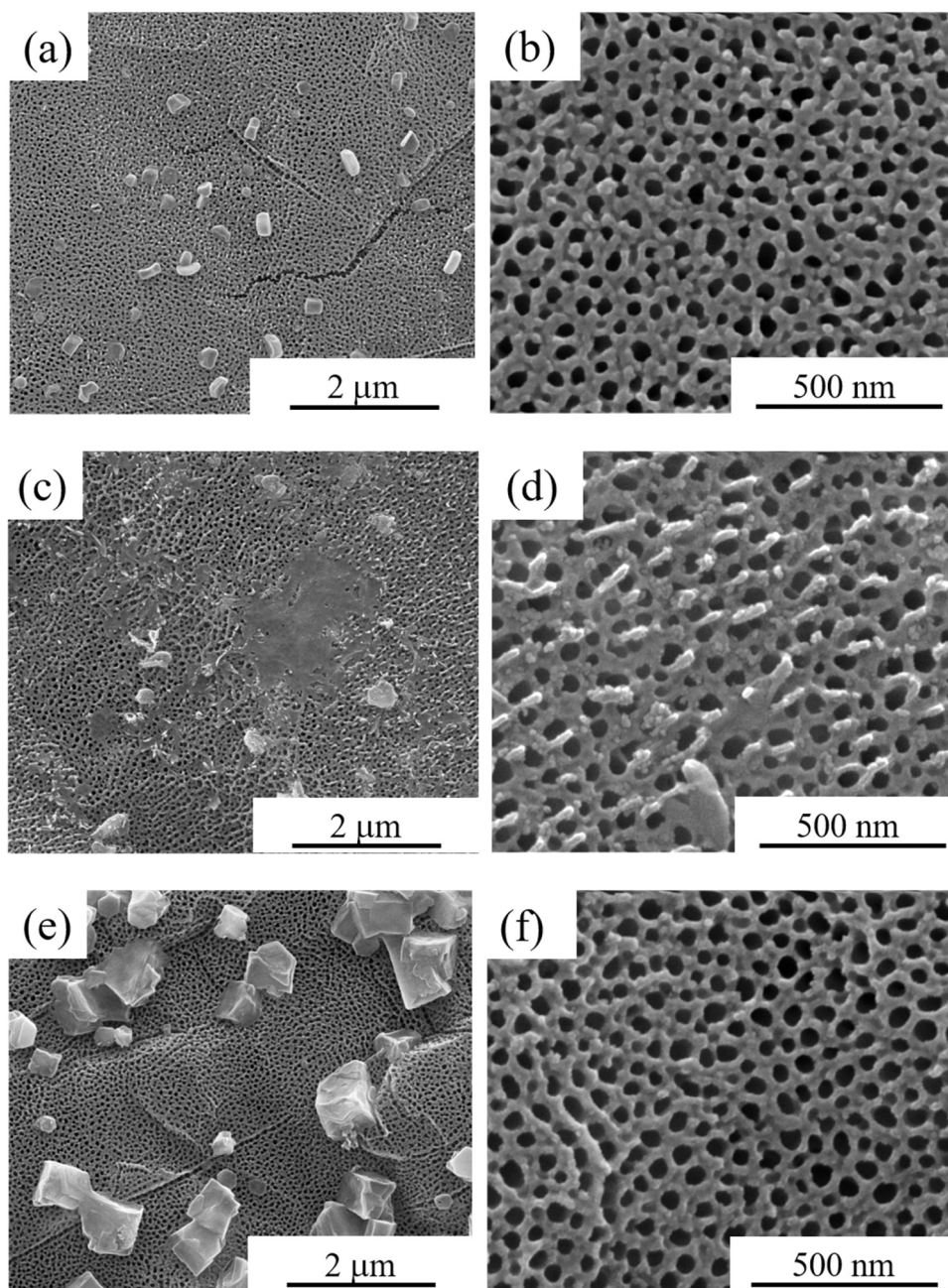


Fig. 2. Surface morphologies of the samples with different Zn contents: (a, b) Zn-TNs-L, (c, d) Zn-TNs-M, and (e, f) Zn-TNs-H.

number of *E. coli* and *S. aureus* colonies were observed in the Petri dish with CP-Ti, indicating the low antibacterial activity of CP-Ti, which is consistent with previous research results [53]. In the samples with Zn-containing coatings, the *E. coli* and *S. aureus* colonies were inhibited. Using CP-Ti as a control, the antibacterial rates of Zn-TNs-L against *E. coli* and *S. aureus* were determined to be 78.35% and 62.42%, respectively. Moreover, the samples showed a higher antibacterial ratio against *E. coli* than against *S. aureus*, mainly owing to the thicker cell walls of *S. aureus* [54].

The antibacterial properties of the samples were mainly attributed to the release of Zn^{2+} from the coatings because Zn^{2+} could combine with proteins to inactivate bacteria, and the ROS produced by the incorporated Zn can inhibit bacterial proliferation [55]. The number of *E. coli* and *S. aureus* colonies both decreased with increasing Zn content, indicating an increase in the antibacterial properties. This could be attributed to the fact that the coating with a higher Zn content released more

Zn^{2+} and generated a larger amount of ROS, resulting in an enhanced antibacterial activity. The antibacterial rates of Zn-TNs-H against *E. coli* and *S. aureus* increased to 97.53% and 96.63%, respectively, suggesting an excellent antibacterial performance compared with that of other samples.

3.6. Cytocompatibility

The absorbance (optical density (OD) value, which reflects the cytotoxicity of the samples) of the MC3T3-E1 cells at 570 nm after being cultured for 24, 96, and 168 h is shown in Fig. 7. The OD values of all the groups increased with increasing cultivation time. After 24 h of co-cultivation, the OD values of all the samples were significantly higher than that of the control. Similar results were obtained after 96 h of culture. Additionally, the OD values of the samples with Zn-containing coatings were all close to those of CP-Ti, without a statistically

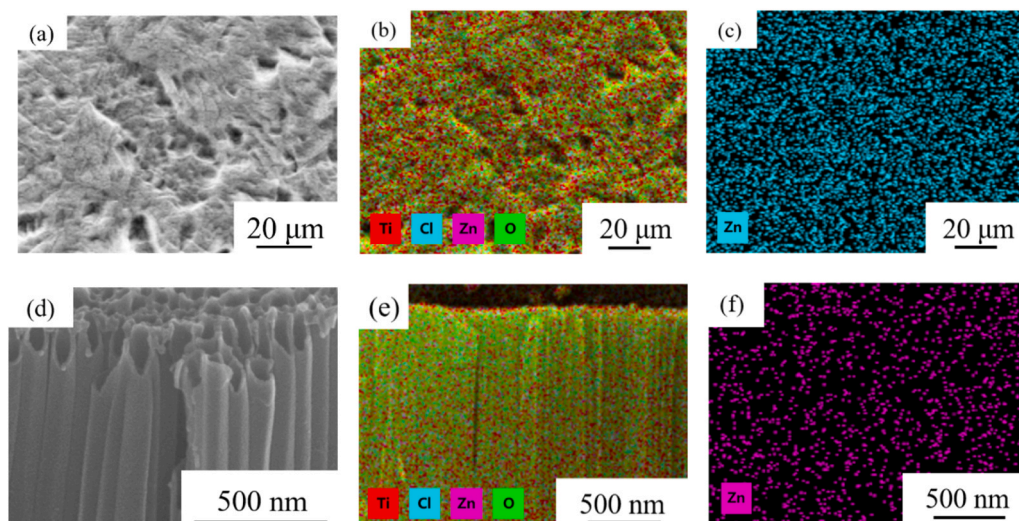


Fig. 3. SEM image, elemental distribution, and Zn maps of Zn-TNs-L: (a, b, c) surface and (d, e, f) side.

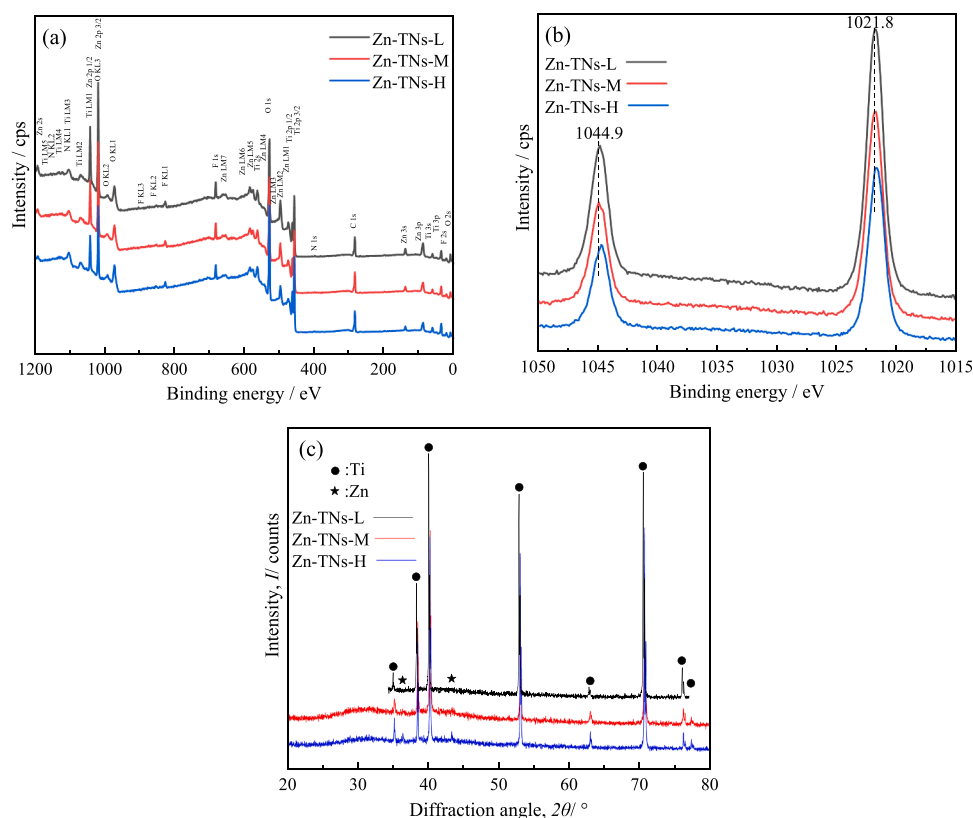


Fig. 4. (a) XPS full spectra, (b) Zn 2p high-resolution spectra, and (c) XRD patterns of the samples.

significant difference. Certain concentrations of Ti and F ions can promote the cell division and proliferation [33,56], which is the main reason for the increase in OD value of the sample compared with that of control. After 168 h of co-cultivation, the OD values of all the samples increased significantly. Statistically significant differences were hardly observed in the OD values of CP-Ti and Zn-TNs-L compared with the control, whereas the OD values of the other groups were significantly lower than that of the control, suggesting that a large amount of Zn ions inhibited the cell proliferation after long time co-culture. The cell viability was expressed as a percentage by calculating the sample-OD-value to the control-OD-value ratio [57], and was an index

to evaluate the cytotoxicity. The cell viabilities of Zn-TNs-M and Zn-TNs-L were 91.7% and 86.8%, respectively, which were both above 80%, and thus they have preferable biological safety (ISO 10993-5).

3.7. Discussion

Thus, a Zn-TNs composite coating was successfully prepared on the surface of CP-Ti, and the adhesion was higher than that of previously reported coatings [58]. Surmenev reported that a magnetron-sputtered hydroxyapatite coating began to fall off at approximately 5.5 N. This significant increase in adhesion can be attributed to the following

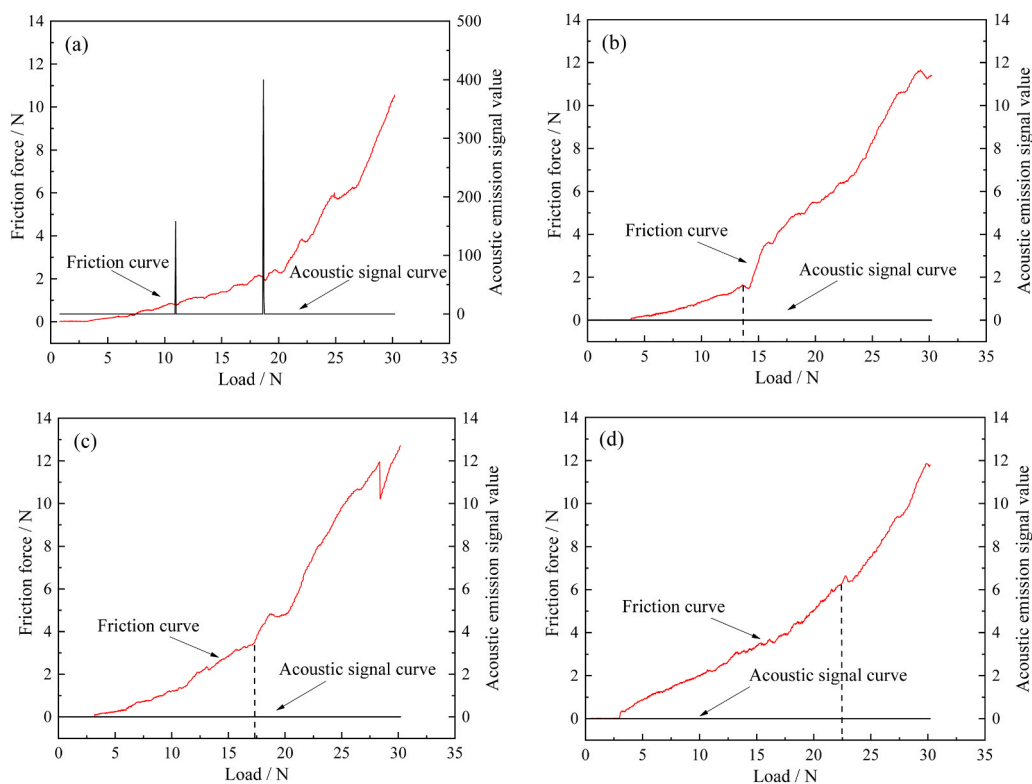


Fig. 5. Friction force and acoustic signal variation curves of (a) TNs, (b) Zn-TNs-L, (c) Zn-TNs-M, and (d) Zn-TNs-H.

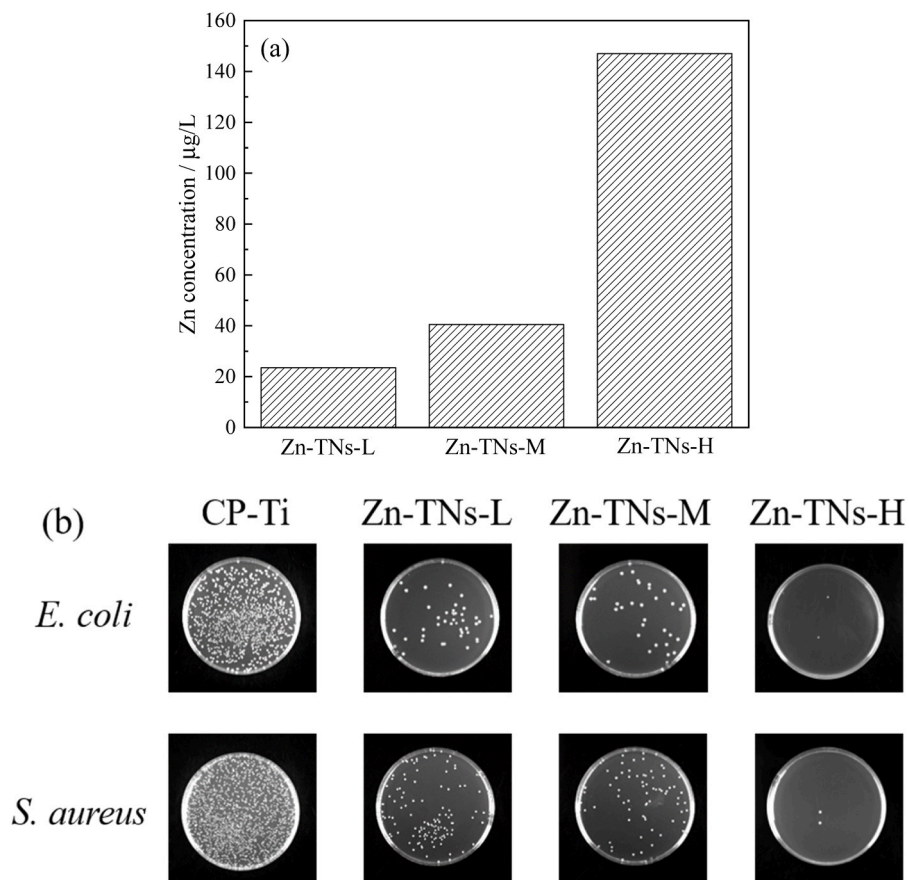


Fig. 6. (a) Release amount of Zn^{2+} ; and (b) optical photos of the plate demonstrating antibacterial performance (*E. coli* and *S. aureus*).

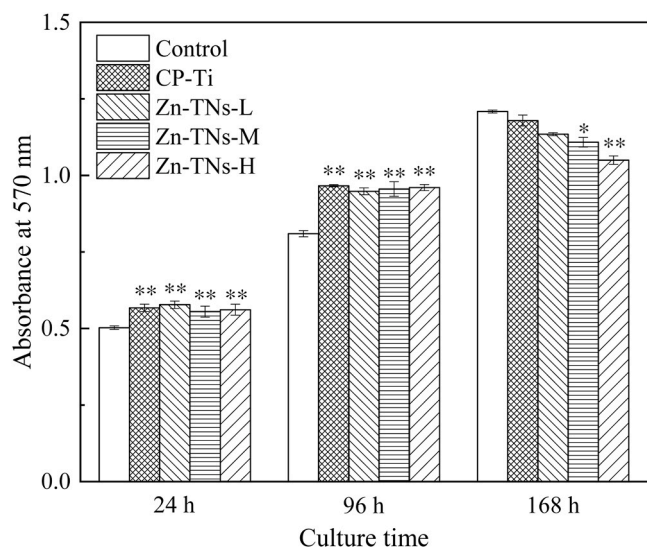


Fig. 7. Absorbance of MC3T3-E1 cells for each sample after 24, 96, and 168 h of culture (* denotes a significant difference at $P < 0.05$ compared with the control, and ** denotes a significant difference at $P < 0.01$ compared with the control).

reasons: (a) the TNs were oxidized in situ on the Ti surfaces, which had a stronger bonding force with the substrate than that of the deposited coating. (b) Zn was uniformly distributed on the top surfaces of the TNs and filled the gaps between the nanotubes. This enhanced the density and roughness of the coatings.

The antimicrobial activity of Zn is mainly due to the release of Zn^{2+} from the implant surface according to a simple reaction: $Zn - 2e \rightarrow Zn^{2+}$. The mechanism of the bactericidal action of Zn^{2+} is as follows. First, Zn^{2+} is released from the coatings and attaches to proteins to inactivate them. Second, Zn^{2+} interacts with the bacterial cell wall, causing structural and permeability changes. Finally, these ions interact with the nucleic acids of bacteria, preventing their migration to other sites [59].

For safety, the release of Zn should be strictly controlled because high concentrations of Zn would cause cytotoxic reactions and inhibit the activity of some proteases [60]. The cytocompatibility tests also indicate excessive Zn^{2+} inhibits cell proliferation. According to the Zn^{2+} releasing results, the Zn^{2+} concentration in the solution is positively correlated with the Zn content of the sample. These results suggest that the Zn content of the samples can be conveniently and effectively regulated by changing the $ZnCl_2$ concentration and deposition time. Therefore, antibacterial activity and cytocompatibility can be controlled by optimizing the deposition parameters to satisfy different application requirements.

After electrical deposition, the porous structure of the TNs was almost completely retained, which is beneficial for osteoblast growth. Previous studies have shown that osteoblasts are the major organization-forming cells involved in osseointegration [61]. Bone matrix deposition on implant surfaces is mainly dependent on competitive adhesion between bacteria and osteoblasts. Osteoblast colonization effectively inhibits bacterial attachment and subsequent biofilm formation on the surface of biomaterials with antimicrobial properties [62]. MC3T3-E1 cells are one of the most commonly used osteoblasts. Based on the antibacterial ratios and cytotoxicities of the samples, coatings containing TNs incorporated with Zn showed high antibacterial activity and acceptable cell viability, suggesting that they have considerable potential for application in bone implants.

4. Conclusions

Zn-containing coatings were prepared on Ti surfaces using TiO_2 nanotubes as the intermediate layer. The following conclusions were

drawn.

(1) Among $ZnCl_2$ concentration in the electrolyte, the deposition time, and deposition temperature, deposition time showed the greatest effect on the Zn content in the electrodeposited samples, whereas the deposition temperature had the smallest effect.

(2) After electrodeposition, Zn was uniformly distributed on the surface and in the tube well of the TiO_2 nanotubes. It existed in the form of a simple substance in the coating and was easily oxidized to ZnO .

(3) The adhesiveness and antibacterial properties were both enhanced with increasing Zn content. The cell proliferation was affected by Zn content, especially after long-time culturing. The cell viabilities of the samples with Zn-containing coatings were all higher than 80%, suggesting they have preferable biological safety.

CRediT authorship contribution statement

Yang Jiawei: Investigation. **Niinomi Mitsuo:** Investigation, Supervision. **Nakano Takayoshi:** Investigation, Supervision. **Li Ming:** Investigation, Writing – original draft, Writing – review & editing. **Li Qiang:** Investigation, Supervision, Writing – original draft, Writing – review & editing.

Declaration of Competing Interest

The authors declare that they have no known competing financial interests or personal relationships that could have appeared to influence the work reported in this paper.

Data availability

Data will be made available on request.

Acknowledgments

This work was partially supported by the Shanghai Engineering Research Center of High-Performance Medical Device Materials (No. 20DZ2255500).

References

- [1] D. Authors, *Titanium in Medicine: Material Science, Surface Science, Engineering, Biological Responses and Medical Applications*, Springer, 2001.
- [2] J. Mouhyi, D.M. Dohan, T. Albrektsson, The peri-implantitis: implant surfaces, microstructure, and physicochemical aspects, *Clin. Implant Dent. Relat. Res.* 14 (2012) 170–183, <https://doi.org/10.1111/j.1708-8208.2009.00244.x>.
- [3] A. Nouri, C. Wen, Introduction to surface coating and modification for metallic biomaterials, in: C. Wen (Ed.), *Surface coating and modification of metallic biomaterials*, Woodhead Publishing, 2015, pp. 3–60, <https://doi.org/10.1016/B978-1-78242-303-4.00001-6>.
- [4] R.S. Khan, A.H. Rather, T.U. Wani, Su Rather, A. Abdal-hay, F.A. Sheikh, A comparative review on silk fibroin nanofibers encasing the silver nanoparticles as antimicrobial agents for wound healing applications, *Mater. Today Commun.* 32 (2022) 103914, <https://doi.org/10.1016/j.mtcomm.2022.103914>.
- [5] G. Pitarresi, F.S. Palumbo, F. Calascibetta, C. Fiorica, M. Di Stefano, G. Giammona, Medicated hydrogels of hyaluronic acid derivatives for use in orthopedic field, *Int J. Pharm.* 449 (2013) 84–94, <https://doi.org/10.1016/j.ijpharm.2013.03.059>.
- [6] M. Maraldi, M. Lisi, G. Moretti, M. Sponchioni, D. Moscatelli, Health care-associated infections: controlled delivery of cationic antiseptics from polymeric excipients, *Int J. Pharm.* 607 (2021) 120956, <https://doi.org/10.1016/j.ijpharm.2021.120956>.
- [7] S. Radin, J.T. Campbell, P. Ducheyne, J.M. Cuckler, Calcium phosphate ceramic coatings as carriers of vancomycin, *Biomaterials* 18 (1997) 777–782, [https://doi.org/10.1016/S0142-9612\(96\)00190-1](https://doi.org/10.1016/S0142-9612(96)00190-1).
- [8] T. Fuchs, R. Stange, G. Schmidmaier, M.J. Raschke, The use of gentamicin-coated nails in the tibia: preliminary results of a prospective study, *Arch. Orthop. Trauma Surg.* 131 (2011) 1419–1425, <https://doi.org/10.1007/s00402-011-1321-6>.
- [9] S. Ferraris, S. Perero, P. Costa, G. Gautier di Confienzo, A. Cochis, L. Rimondini, F. Renaux, E. Vernè, M. Ferraris, S. Spriano, Antibacterial inorganic coatings on metallic surfaces for temporary fixation devices, *Appl. Surf. Sci.* 508 (2020) 144707, <https://doi.org/10.1016/j.apsusc.2019.144707>.
- [10] L. Zhao, P.K. Chu, Y. Zhang, Z. Wu, Antibacterial coatings on titanium implants, *J. Biomed. Mater. Res. B Appl. Biomater.* 91b (2010) 470–480, <https://doi.org/10.1002/jbm.b.31463>.

- [11] A. Ince, N. Schutze, C. Hendrich, F. Jakob, J. Eulert, J.F. Lohr, Effect of polyhexanide and gentamycin on human osteoblasts and endothelial cells, *Swiss Med. Wkly* 137 (2007) 139–145, <https://doi.org/10.4414/smww.2007.11434>.
- [12] L.G. Harris, L. Mead, E. Muller-Oberlander, R.G. Richards, Bacteria and cell cytocompatibility studies on coated medical grade titanium surfaces, *J. Biomed. Mater. Res A* 78A (2006) 50–58, <https://doi.org/10.1002/jbm.a.30611>.
- [13] A. Rodriguez-Conteras, D. Torres, B. Rafik, M. Ortiz-Hernandez, M.P. Ginebra, J. A. Calero, J.M. Manero, E. Ruperez, Bioactivity and antibacterial properties of calcium- and silver-doped coatings on 3D printed titanium scaffolds, *Surf. Coat. Technol.* 421 (2021) 127476, <https://doi.org/10.1016/j.surfcoat.2021.127476>.
- [14] X. Chang, X. Wang, J. Li, M. Shang, S. Niu, W. Zhang, Y. Li, Z. Sun, J. Gan, W. Li, M. Tang, Y. Xue, Silver nanoparticles induced cytotoxicity in HT22 cells through autophagy and apoptosis via PI3K/AKT/mTOR signaling pathway, *Ecotoxicol. Environ. Saf.* 208 (2021) 111696, <https://doi.org/10.1016/j.ecoenv.2020.111696>.
- [15] M. Yamaguchi, H. Oishi, Y. Suketa, Zinc stimulation of bone protein synthesis in tissue culture. Activation of aminoacyl-tRNA synthetase, *Biochem. Pharm.* 37 (1988) 4075–4080, [https://doi.org/10.1016/0006-2952\(88\)90098-6](https://doi.org/10.1016/0006-2952(88)90098-6).
- [16] H.J. Seo, Y.E. Cho, T. Kim, H.I. Shin, I.S. Kwun, Zinc may increase bone formation through stimulating cell proliferation, alkaline phosphatase activity and collagen synthesis in osteoblastic MC3T3-E1 cells, *Nutr. Res. Pr.* 4 (2010) 356–361, <https://doi.org/10.4162/nrp.2010.4.5.356>.
- [17] M. Hashizume, M.J.M. Yamaguchi, C. Biochemistry, Stimulatory effect of β -alanine-L-histidinato zinc on cell proliferation is dependent on protein synthesis in osteoblastic MC3T3-E1 cells, *Mol. Cell Biochem.* 122 (1993) 59–64, <https://doi.org/10.1007/BF00925737>.
- [18] X.P. Wang, A. Ito, Y. Sogo, X. Li, A. Oyane, Zinc-containing apatite layers on external fixation rods promoting cell activity, *Acta Biomater.* 6 (2010) 962–968, <https://doi.org/10.1016/j.actbio.2009.08.038>.
- [19] K. Yusa, O. Yamamoto, M. Fukuda, S. Koyota, Y. Koizumi, T. Sugiyama, In vitro prominent bone regeneration by release zinc ion from Zn-modified implant, *Biochem. Biophys. Res. Commun.* 412 (2011) 273–278, <https://doi.org/10.1016/j.bbrc.2011.07.082>.
- [20] N. Dukstiene, D. Sinkeviciute, A. Guobiene, Morphological, structural and optical properties of MoO₂ films electrodeposited on SnO₂/glass plate, *Cent. Eur. J. Chem.* 10 (2012) 1106–1118, <https://doi.org/10.2478/s11532-012-0012-7>.
- [21] A. Aynaou, B. Youbi, M.A. Himi, Y. Lghazi, J. Bahar, C. El Haimer, A. Ouedrhiri, A. Himi, Electropolymerization investigation of polyaniline films on ITO substrate, *Mater. Today Proc.* 66 (2022) 335–340, <https://doi.org/10.1016/j.matpr.2022.05.437>.
- [22] C. El Haimer, Y. Lghazi, J. Bahar, B. Youbi, M.A. Himi, A. Ouedrhiri, A. Aynaou, I. Bimaghra, Investigation of nucleation and growth mechanism of selenium electrodeposited on ITO substrate, *Mater. Today Proc.* 66 (2022) 37–44, <https://doi.org/10.1016/j.matpr.2022.03.107>.
- [23] B. Makurat-Kasprolewicz, A. Ossowska, Recent advances in electrochemically surface treated titanium and its alloys for biomedical applications: A review of anodic and plasma electrolytic oxidation methods, *Mater. Today Commun.* 34 (2023) 105425, <https://doi.org/10.1016/j.mtcomm.2023.105425>.
- [24] L. Fan, Y. Zhang, R. Hu, C. Lin, W. Shi, Z. Tian, Strontium substituted octacalcium phosphate coatings by electrochemical deposition and their dose-dependent bioactivities, *Mater. Lett.* 272 (2020) 127844, <https://doi.org/10.1016/j.matlet.2020.127844>.
- [25] Y. Say, B. Aksakal, B. Dikici, Effect of hydroxyapatite/SiO₂ hybride coatings on surface morphology and corrosion resistance of REX-734 alloy, *Ceram. Int.* 42 (2016) 10151–10158, <https://doi.org/10.1016/j.ceramint.2016.03.127>.
- [26] L.Z. Zhao, L. Liu, Z.F. Wu, Y.M. Zhang, P.K. Chu, Effects of micropitted/nanotubular titania topographies on bone mesenchymal stem cell osteogenic differentiation, *Biomaterials* 33 (2012) 2629–2641, <https://doi.org/10.1016/j.biomaterials.2011.12.024>.
- [27] N. Wang, H.Y. Li, W.L. Lu, J.H. Li, J.S. Wang, Z.T. Zhang, Y.R. Liu, Effects of TiO₂ nanotubes with different diameters on gene expression and osseointegration of implants in minipigs, *Biomaterials* 32 (2011) 6900–6911, <https://doi.org/10.1016/j.biomaterials.2011.06.023>.
- [28] S. Shanmugam, B. Gopal, Antimicrobial and cytotoxicity evaluation of aliovalent substituted hydroxyapatite, *Appl. Surf. Sci.* 303 (2014) 277–281, <https://doi.org/10.1016/j.apsusc.2014.02.166>.
- [29] E.B. Aydin, G. Sigircik, H.A.M. Takci, Antimicrobial properties and corrosion behavior of TiO₂-NTs electrodes modified with Ag and ZnO nanorod in simulated body fluid solution, *J. Mol. Struct.* 1240 (2021) 130569, <https://doi.org/10.1016/j.molstruc.2021.130569>.
- [30] S. Ahmadi, I. Mohammadi, S.K. Sadrnezhad, Hydroxyapatite based and anodic Titania nanotube biocomposite coatings: Fabrication, characterization and electrochemical behavior, *Surf. Coat. Technol.* 287 (2016) 67–75, <https://doi.org/10.1016/j.surfcoat.2015.12.062>.
- [31] H.B. Wu, X.Y. Zhang, Z.H. Geng, Y. Yin, R.Q. Hang, X.B. Huang, X.H. Yao, B. Tang, Preparation, antibacterial effects and corrosion resistant of porous Cu-TiO₂ coatings, *Appl. Surf. Sci.* 308 (2014) 43–49, <https://doi.org/10.1016/j.apsusc.2014.04.081>.
- [32] S.A. Alves, A.L. Rossi, A.R. Ribeiro, J. Werckmann, J.P. Celis, L.A. Rocha, T. Shokuhfar, A first insight on the bio-functionalization mechanisms of TiO₂ nanotubes with calcium, phosphorous and zinc by reverse polarization anodization, *Surf. Coat. Technol.* 324 (2017) 153–166, <https://doi.org/10.1016/j.surfcoat.2017.05.073>.
- [33] S.A. Alves, S.B. Patel, C. Sukotjo, M.T. Mathew, P.N. Filho, J.P. Celis, L.A. Rocha, T. Shokuhfar, Synthesis of calcium-phosphorous doped TiO₂ nanotubes by anodization and reverse polarization: a promising strategy for an efficient biofunctional implant surface, *Appl. Surf. Sci.* 399 (2017) 682–701, <https://doi.org/10.1016/j.apsusc.2016.12.105>.
- [34] B.G. Bibby, M.J. Van Kesteren, The effect of fluorine on mouth bacteria, *J. Dent. Res.* 19 (1940) 391–401, <https://doi.org/10.1177/00220345400190040601>.
- [35] J.H. Li, W.J. Zhang, Y.Q. Qiao, H.Q. Zhu, X.Q. Jiang, X.Y. Liu, C.X. Ding, Chemically regulated bioactive ion delivery platform on a titanium surface for sustained controlled release, *J. Mater. Chem. B* 2 (2014) 283–294, <https://doi.org/10.1039/c3tb21102a>.
- [36] A. Ghicov, H. Tsuchiya, R. Hahn, J.M. Macak, A.G. Munoz, P. Schmuki, TiO₂ nanotubes: H⁺ insertion and strong electrochromic effects, *Electrochem Commun.* 8 (2006) 528–532, <https://doi.org/10.1016/j.elecom.2006.01.015>.
- [37] B. Feng, X. Chu, J. Chen, J. Wang, X. Lu, J. Weng, Hydroxyapatite coating on titanium surface with titania nanotube layer and its bond strength to substrate, *J. Porous Mat.* 17 (2010) 453–458, <https://doi.org/10.1007/s10934-009-9307-2>.
- [38] S. Khanmohammadi, M. Ojaghi-Ilkchi, M. Farrokhi-Rad, Development of bioglass coating reinforced with hydroxyapatite whiskers on TiO₂ nanotubes via electrophoretic deposition, *Ceram. Int.* 47 (2021) 1333–1343, <https://doi.org/10.1016/j.ceramint.2020.08.255>.
- [39] L.W. Lv, Y.S. Liu, P. Zhang, X. Zhang, J.Z. Liu, T. Chen, P.L. Su, H.Y. Li, Y.S. Zhou, The nanoscale geometry of TiO₂ nanotubes influences the osteogenic differentiation of human adipose-derived stem cells by modulating H3K4 trimethylation, *Biomaterials* 39 (2015) 193–205, <https://doi.org/10.1016/j.biomaterials.2014.11.002>.
- [40] Y. Wang, S. Zhao, G. Li, S. Zhang, R. Zhao, A. Dong, R. Zhang, Preparation and in vitro antibacterial properties of anodic coatings co-doped with Cu, Zn, and P on a Ti–6Al–4V alloy, *Mater. Chem. Phys.* 241 (2020) 122360, <https://doi.org/10.1016/j.matchemphys.2019.122360>.
- [41] G. Lian, Z. Liu, Y. Zhang, L. Que, C. Chen, K. Yue, Grey relational analysis-based composite coating property optimization fabricated by laser cladding, *Int. J. Adv. Manuf. Technol.* 120 (2022) 7985–7996, <https://doi.org/10.1007/s00170-022-09305-x>.
- [42] J.H. Zhou, Y. Han, S.M. Lu, Direct role of interrod spacing in mediating cell adhesion on Sr-HA nanorod-patterned coatings, *Int. J. Nanomed.* 9 (2014) 1243–1260, <https://doi.org/10.2147/IJN.S58236>.
- [43] C. Wagner, W.M. Riggs, L.E. Davis, J.F. Moulder, G.E. Muilenberg, *Handbook of X-ray photoelectron spectroscopy*, Phys. Electron. Div. Minn. (1979).
- [44] A. Ali, Y.W. Chiang, R.M. Santos, X-ray diffraction techniques for mineral characterization: a review for engineers of the fundamentals, applications, and research directions, *Minerals* 12 (2022) 205, <https://doi.org/10.3390/min12020205>.
- [45] R. Gobeira, P.S. Esbah Tabaei, R. Morent, N. De Geyter, Chemical characterization of plasma-activated polymeric surfaces via XPS analyses: a review, *Surf. Interfaces* 31 (2022) 102087, <https://doi.org/10.1016/j.surfint.2022.102087>.
- [46] R. Kumar, A. Umar, G. Kumar, H.S. Nalwa, Antimicrobial properties of ZnO nanomaterials: a review, *Ceram. Int.* 43 (2017) 3940–3961, <https://doi.org/10.1016/j.ceramint.2016.12.062>.
- [47] J. Ye, B. Li, M. Li, Y.F. Zheng, S.L. Wu, Y. Han, ROS induced bactericidal activity of amorphous Zn-doped titanium oxide coatings and enhanced osseointegration in bacteria-infected rat tibias, *Acta Biomater.* 107 (2020) 313–324, <https://doi.org/10.1016/j.actbio.2020.02.036>.
- [48] A. Krainoi, V. Prasert, P. Kesakomol, P. Thongdee, S. Nitchaphanit, N. Sungsirin, T. Boonsiri, V. Watanaveeradej, K. Ounjai, Y. Nakaramontri, Effect of modified zinc oxide nanoparticles on enhancement of mechanical, thermal and antibacterial properties of disinfectant natural rubber latex foams, *Mater. Today Commun.* 35 (2023) 105601, <https://doi.org/10.1016/j.mtcomm.2023.105601>.
- [49] H.F. Li, X.H. Xie, Y.F. Zheng, Y. Cong, F.Y. Zhou, K.J. Qiu, X. Wang, S.H. Chen, L. Huang, L. Tian, L. Qin, Development of biodegradable Zn-1X binary alloys with nutrient alloying elements Mg, Ca and Sr, *Sci. Rep.* 5 (2015) 10719, <https://doi.org/10.1038/srep10719>.
- [50] G.-X. Gao, Y.-B. Tan, J. Sun, Y.-S. Zheng, Z.-H. Jin, Effect of contents of Zn (MAA)2 and Mg (MAA)2 on insulation/metal adhesion, *J. Solid Rocket Technol. (China)* 32 (2009) 344–347, <https://doi.org/10.1145/1651587.1651601>.
- [51] W.H. Song, J.Y. Zhang, J. Guo, J.H. Zhang, F. Ding, L.Y. Li, Z.T. Sun, Role of the dissolved zinc ion and reactive oxygen species in cytotoxicity of ZnO nanoparticles, *Toxicol. Lett.* 199 (2010) 389–397, <https://doi.org/10.1016/j.toxlet.2010.10.003>.
- [52] C.Y. Ning, X.L. Wang, L.H. Li, Y. Zhu, M. Li, P. Yu, L. Zhou, Z.N. Zhou, J.Q. Chen, G. X. Tan, Y. Zhang, Y.J. Wang, C.B. Mao, Concentration ranges of antibacterial cations for showing the highest antibacterial efficacy but the least cytotoxicity against mammalian cells: implications for a new antibacterial mechanism, *Chem. Res. Toxicol.* 28 (2015) 1815–1822, <https://doi.org/10.1021/acs.chemrestox.5b00258>.
- [53] L.H. Mei, H.Y. Wang, W. Wang, L.P. Tong, H.B. Pan, C.S. Ruan, Q.L. Ma, M.Y. Liu, H.L. Yang, L. Zhang, Y.C. Cheng, Y.M. Zhang, L.Z. Zhao, P.K. Chu, Antibacterial effects and biocompatibility of titanium surfaces with graded silver incorporation in titania nanotubes, *Biomaterials* 35 (2014) 4255–4265, <https://doi.org/10.1016/j.biomaterials.2014.02.005>.
- [54] N. Murugan, C. Murugan, A.K. Sundramoorthy, In vitro and in vivo characterization of mineralized hydroxyapatite/polycaprolactone-graphene oxide based bioactive multifunctional coating on Ti alloy for bone implant applications, *Arab J. Chem.* 11 (2018) 959–969, <https://doi.org/10.1016/j.arabjc.2018.03.020>.
- [55] H. Hu, W. Zhang, Y. Qiao, X. Jiang, X. Liu, C. Ding, Antibacterial activity and increased bone marrow stem cell functions of Zn-incorporated TiO₂ coatings on titanium, *Acta Biomater.* 8 (2012) 904–915, <https://doi.org/10.1016/j.actbio.2011.09.031>.
- [56] C. Li, Q.Y. Li, Y. Qian, F.J. C. L. Tang, Effect of titanium ions on the proliferation and intracellular calcium concentration in Jurkat T cells, *J. Guangxi Med. Univ.*

- (China) 34 (2017) 654–658, <https://doi.org/10.16190/j.cnki.45-1211/r.2017.05.004>.
- [57] L. Fan, W. Sun, Y. Zou, Q.-q Xu, R.-C. Zeng, J. Tian, Enhanced corrosion resistance, antibacterial activity and biocompatibility of gentamicin-montmorillonite coating on Mg alloy-in vitro and in vivo studies, *J. Mater. Sci. Technol.* 111 (2022) 167–180, <https://doi.org/10.1016/j.jmst.2021.08.089>.
- [58] R.A. Surmenev, I. Grubova, E.C. Neyts, A.D. Teresov, M.A.J.S. Surmeneva, Interfaces, ab initio calculations and a scratch test study of RF-magnetron sputter deposited hydroxyapatite and silicon-containing hydroxyapatite coatings, *Surf. Interfaces* 21 (2020) 100727, <https://doi.org/10.1016/j.surfin.2020.100727>.
- [59] Q. Bi, X. Song, Y. Chen, Y. Zheng, P. Yin, T. Lei, Zn-HA/Bi-HA biphasic coatings on titanium: fabrication, characterization, antibacterial and biological activity, *Colloids Surf. B Biointerfaces* 189 (2020) 110813, <https://doi.org/10.1016/j.colsurfb.2020.110813>.
- [60] T.D. Zaveri, N.V. Dolgova, B.H. Chu, J.Y. Lee, J.E. Wong, T.P. Lele, F. Ren, B. G. Keselowsky, Contributions of surface topography and cytotoxicity to the macrophage response to zinc oxide nanorods, *Biomaterials* 31 (2010) 2999–3007, <https://doi.org/10.1016/j.biomaterials.2009.12.055>.
- [61] G. Jin, H. Cao, Y. Qiao, F. Meng, H. Zhu, X. Liu, Osteogenic activity and antibacterial effect of zinc ion implanted titanium, *Colloids Surf. B Biointerfaces* 117 (2014) 158–165, <https://doi.org/10.1016/j.colsurfb.2014.02.025>.
- [62] L.Y. Chu, Y. Yang, S.B. Yang, Q.M. Fan, Z.F. Yu, X.L. Hu, T.D. James, X.P. He, T. T. Tang, Preferential colonization of osteoblasts over co-cultured bacteria on a bifunctional biomaterial surface, *Front Microbiol* 9 (2018) 2219, <https://doi.org/10.3389/fmicb.2018.02219>.